Mathematical Characterization of One-Dimensional Compression, Undrained and Drained Sand Behavior in Axisymmetric Tests at High Pressures

Eulalio Juárez-Badillo
Graduate School of Engineering, National University of Mexico

2011 Pan-Am CGS Geotechnical Conference

ABSTRACT
The theoretical general equations of compressibility, stress-strain relations for geomaterials provided by the principle of natural proportionality are applied to describe the compression of sands to axial stresses up to 850.0 MPa; three different initial densities of quartz, Cambria, and gypsum sands are considered. Also the undrained sand behavior in compression and extension tests with initial confining pressures up to 68.9 MPa and also the drained sand behavior in compression and extension tests with initial confining pressures up to 52.0 MPa are considered.

RESUMEN
Las ecuaciones teóricas de compresibilidad y las relaciones esfuerzo-deformación para geomateriales que establece el principio de proporcionalidad natural, se aplicaron para describir la compresibilidad de arenas bajo cargas axiales de hasta 850.9 MPa; se consideraron probetas con tres diferentes densidades iniciales de arena de cuarzo, Cambria y gypsum. También se consideró el comportamiento no-drenado de la arena en pruebas de compresión y extensión con confinamientos iniciales hasta de 68.0 MPa, así como el comportamiento drenado en pruebas de compresión y extensión, utilizando confinamientos iniciales de hasta 52.0 MPa.

1 INTRODUCTION

"One-Dimensional Compression of Sands at High Pressures" is the title of a paper by Yamamuro J. A et al. (1996), "Undrained Sand Behavior in Axisymmetric Tests at High Pressures" is the title of a paper by Lade P. V. and Yamamuro J. A. (1996) and "Drained Sand Behavior in Axisymmetric Tests at High Pressures" is the title of a paper by Yamamuro J. A. and Lade P.V. (1996), all published in the Journal of Geotechnical Engineering, that the author just found and after reading them, he was very interested in applying the general theoretical equations provided by the principle of natural proportionality to describe the experimental data. The result is the subject of this paper. The author highly suggest to the readers of this paper to read first the above mentioned papers for a complete information of these tests. Some information follows.

For the first paper "One-Dimensional Compression of Sands at High Pressures":

2 TESTING EQUIPMENT

"A vertical cross-sectional view of the thick-walled containment cell and piston is shown in Figure. 1. The axisymmetric test specimen diameter is 3.81 cm (1.5 in). The specimen height can be variable, but a specimen height of approximately 7.62 cm (3.0 in) was generally used."

3 SANDS USED IN TESTING

"To understand the behavior of sand under high-pressure, one-dimensional compression, three sands of different mineral hardnesses were used. The hardest sand was a uniform, angular quartz sand (Mohs' hardness of 7) with grain sizes ranging from 0.60 to 1.70 mm, and with a minimum void ratio of 0.66 and a maximum void ratio of 1.07. The softest sand was a uniform gypsum sand (Mohs' hardness of 2), with grain sizes that ranged from 0.075 to 1.18 mm, and with a minimum void ratio of 0.70 and a maximum void ratio of 0.97. The sand of intermediate hardness was a rounded, uniform Cambria sand with grain sizes that ranged from 0.83 and 2.00 mm, and with a minimum void ratio of 0.49 and a maximum void ratio of 0.78. The hardness of Cambria sand cannot be defined by one value, since it is composed of many different mineral constituents, which vary in hardness between the hardnesses of quartz and gypsum. Each sand was tested at three different initial void ratios."

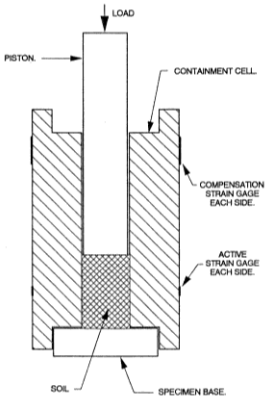

Figure 1. Vertical Cross-Secttion of Assembled One-Dimensional Compression Testing System Including Strain Gauge Locations and Specimen (from Yamamuro et al. 1996)

"The different sands were dry-pluviated from various heights to achieve the desired densities. Tests were performed in both dry and wet states. At high stress levels, the presence of water in the sand had no apparent effects."

4 STRESS-STRAIN BEHAVIOR

"The loading and unloading axial stress-strain curves for quartz, Cambria, and gypsum sands are shown in Figures. 2, 3, and 4, respectively (Yamamuro. 1993; Bopp. 1994). Since the one-dimensional tests is a fully confined test, there is no failure condition. The soil densifies, resulting in continually increasing stiffness, as shown in the figures. Most tests were terminated at the maximum capacity of the loading system. Specimens with lower initial densities experienced larger axial strains at maximum stress condition than did denser specimens, because the additional axial strains are required to reach higher densities at high stress levels. The shapes of high stress portions of the stress-strain curves appear almost identical."

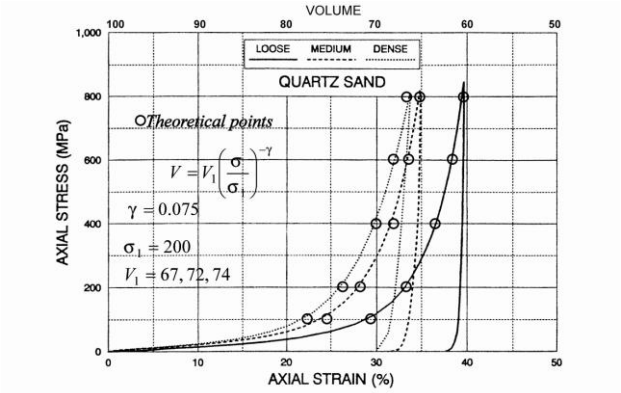

Figure 2. Axial Stress Related to Axial Strain for One-Dimensional Compression Tests on Quartz Sand (from Yamamuro et al. 1996)

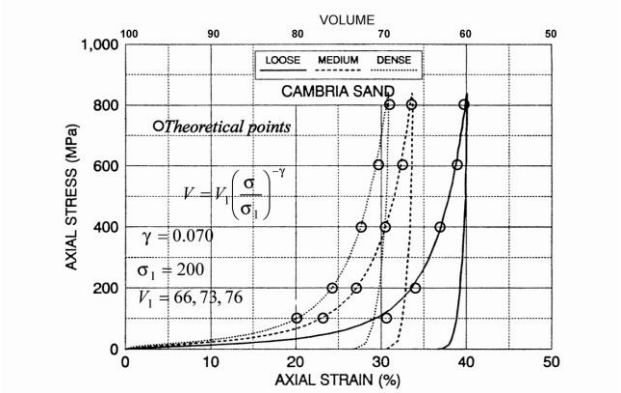

Figure 3. Axial Stress Related to Axial Strain for One-Dimensional Compression Tests on Cambria Sand (from Yamamuro et al. 1996)

"The void ratios plotted against axial stress for quartz, Cambria, and gypsum sands are shown in Figures 5, 6, and 7, respectively. Three initial densities were used for each sand. The effectiveness of lubrication can observed on these figures. Figure 5 displays results from nonlubricated tests (full friction) and lubricated tests (reduced friction) on quartz sand. It can be seen that the reduced-friction test on medium dense quartz sand crosses over the curve obtained from the dense quartz to achieve a lower overall void ratio at the maximum stress condition. It is also observed that the two full-friction tests join together near the maximum stress."

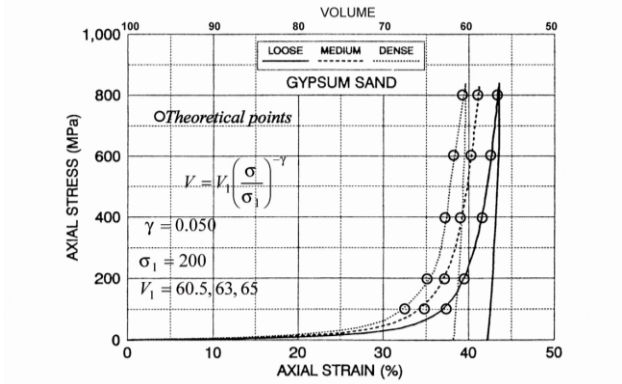

Figure 4. Axial Stress Related to Axial Strain for One-Dimensional Compression Tests on Gypsum Sand (from Yamamuro et al. 1996)

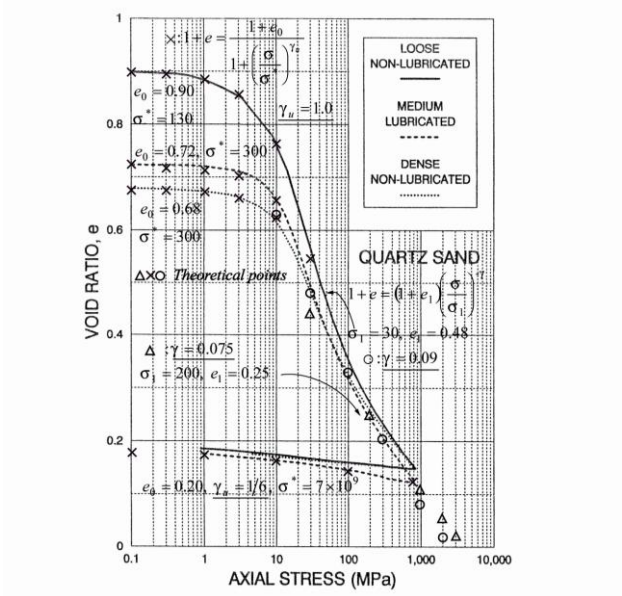

Figure 5. Void Ratio to Axial Stress for One-Dimension Compression Tests on Quartz Sand (from Yamamuro et al. 1996)

"Figures 6 and 7 indicate results from tests in which lubrication (reduce friction) was used in all tests. Within the range of experimental scatter, these results indicate that the different initial void-ratio curves tend to join and stay together. It may be concluded, therefore, that the effect of the initial void ratio in sands is eliminated at high stress magnitudes. The magnitude of stress at which the curves join each other appears to be related to the mineral hardness. Mineralogically harder sands have a higher value of this stress than softer grained sands. The minimum void ratios achieved for the same maximum axial stress also appear to be directly related to the value of mineral hardness. The minimum void ratio of the hard quartz sand was about 0.13, while Cambria sand achieved a minimum void ratio of about 0.07. The soft gypsum sand experienced the highest void ratio reduction, down to approximately 0.02 at the maximum stress."

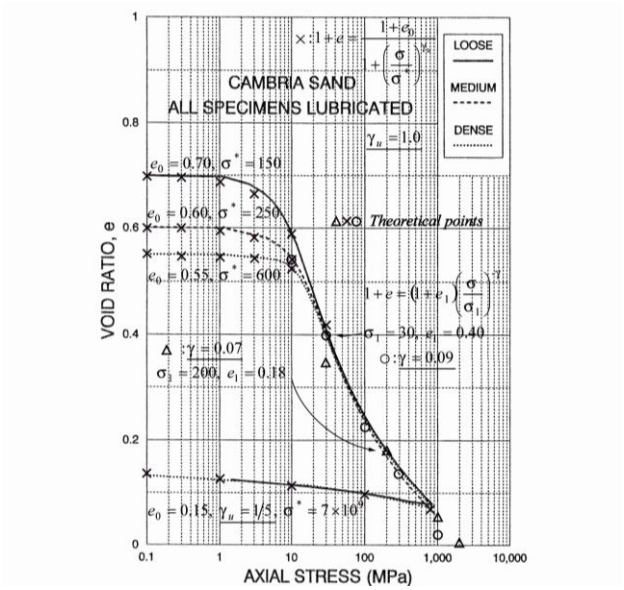

Figure 6. Void Ratio to Axial Stress for One-Dimenssion Compression Tests on Cambria Sand (from Yamamuro et al. 1996)

For the second paper "Undrained Sand Behavior in Axisymmetric Tests at High Pressures"

4.1 Behavior in compression

"Undrained triaxial compression tests were performed with initial confining pressures between 6.4 and 68.9 MPa. The tests consisted of drained isotropic compression followed by undrained shearing under axial strain control. The total confining pressure was maintained constant throughout shearing. Induced pore pressures were measured with a pressure transducer attached to the base of the triaxial cell."

"It was not possible to perform undrained compression tests with initial confining pressures lower than approximately 6 MPa, because the relatively large grain size of the Cambia sand (D_{50} = 1.66 mm. C_u = 1.30) would create membrane penetration effects, thereby affecting the pore pressure response (Lade and Hernandez, 1977). For Cambria sand it has been shown that membrane penetration effects cease at an effective confining pressure of approximately 2 MPa (Yamamuro and Lade. 1993a)."

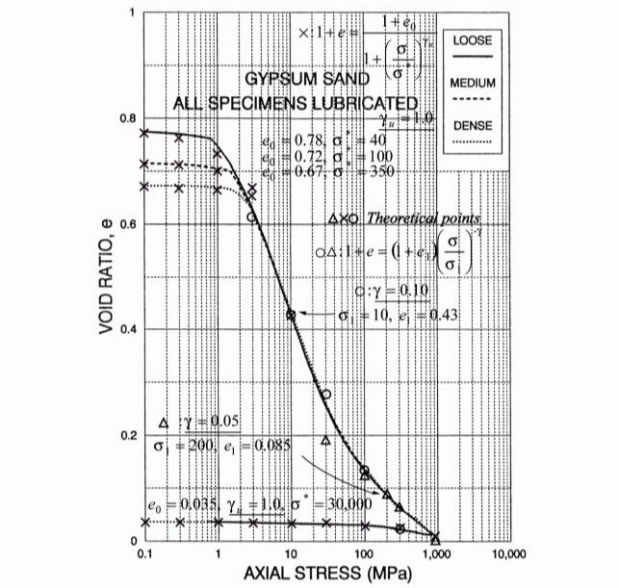

Figure 7. Void Ratio Related to Axial Stress for One-Dimenssion Compression Tests on Gypsum Sand (from Yamamuro et al. 1996)

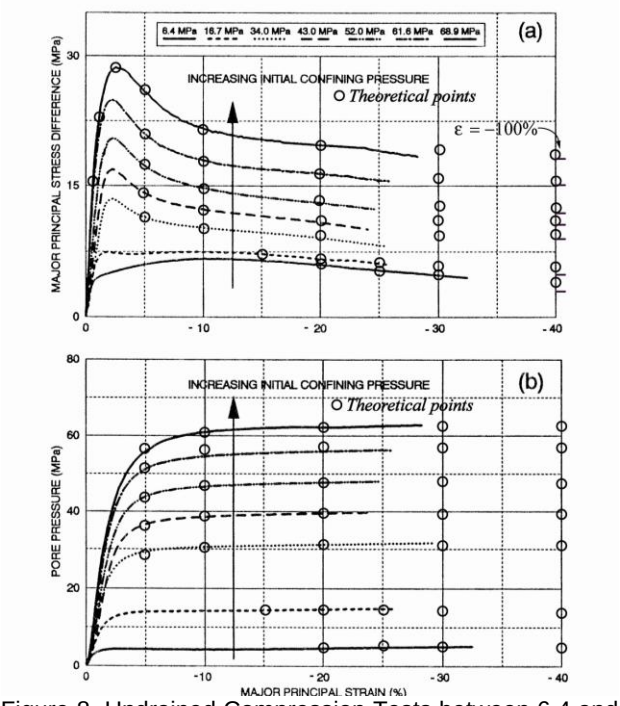

Figure 8. Undrained Compression Tests between 6.4 and 68.9 Mpa Initial Confining Pressures on Dense Cambria Sand: (a) Principal Stress Difference; and (b) Pore Pressure Relationa (from Lade and Yamamuro. 1996)

"In the undrained test with initial confining pressure of 6.4 MPa the effective confining pressure barely reaches down to about 2 MPa. The principal stress difference (σ_1 - σ_3) and the pore pressure are plotted against the major principal strain (ε_1) in Figure 8. The principal stress differences shown on Figure 8 (a) indicate steeper initial slopes of the stress-strain curve as the initial confining pressures increase. At low initial confining pressures, such as in the 6.4MPa test, the maximum principal stress difference occurs at large strains. The test at 16.7 MPa shows the stress difference increasing to a peak, followed by a decrease, but then it rises again to its maximum value at failure. This occurs as a result of the volume change tendency of the specimen. After the first peak is reached, the drop in the principal stress difference is caused by the tendency of the specimen to compress volumetrically, causing the pore pressure to rise, thus decreasing the effective stress. At larger strains, the effective confining pressure has declined sufficiently to allow the specimen to exhibit volumetrically dilatant tendencies, causing the pore pressures to drop, thereby increasing the effective stress. The pore pressure drop is not readily apparent in Figure 8 (b), but is clearly indicated in Figure 2 (Lade and Yamamuro. 1996, not included in this paper). This in turn permits the stress difference to increase. Eventually, the specimen reaches failure, after which the principal stress difference decreases with additional shearing."

"The pore pressures shown in Figure 8 (b) indicate that all tests display tendencies for overall net compressive volumetric behavior, since the induced pore pressures are all positive. As the initial confining pressure is increased above the 16.7 MPa test, the value of the maximum principal stress difference increases, but it occurs at very low strain levels, as indicated in Figure 8 (a). Large, quickly developing pore pressures cause a rapid decrease in the effective confining pressure in the specimen, resulting in the principal stress difference peaking soon after shearing begins. As the initial confining pressure increases, the strain to the maximum principal stress difference increases slightly. Beyond the peak, the magnitude of the principal stress difference declines with increasing strain until the end of the test. This continuing decline in stress difference is caused by the pore pressures, which continue to increase with additional shearing."

"Close inspection of the pore pressure curves associated with the higher confining pressure tests in Figure 8 (b) indicates a slight hesitation in the pore pressure development immediately at the onset of shearing. This is the same effect causing the slight delay in the volume change response observed in high-pressure drained tests (Yamamuro and Lade. 1996). This was the result of volumetric creep occurring between isotropic consolidation and the start of shearing."

4.2 Behavior in extension

"A series of undrained uniform strain triaxial extension tests were performed with initial confining pressures between 12.0 and 52.0 MPa. The tests consisted of drained isotropic compression followed by shearing under axial strain control."

"The occurrence of train localization in extension was a major consideration. The inherent instability in the extension test caused by the concentration of stresses at inhomogeneities (either material or geometric) in the specimen inevitably creates strain localization in the form of necking. To inhibit the development of strain localization in the specimen during shearing, a method was developed to enforce uniform strains in extension. The resulting method is discussed in the companion article (Yamamuro and Lade, 1996) and by Yamamuro (1993). The differences between uniform strain extension tests and tests experiencing strain localization were discussed by Yamamuro and Lade (1995)."

"The principal stress differences in extension are shown on Figure 9(a) plotted against the radial strain ε_1. They indicate a consistent pattern with increasing initial slopes of the stress-strain curves and increasing maximum principal stress differences with increasing confining pressure, similar to the undrained compression tests (Figure 2)." (Lade and Yamamuro. 1996, not included in this paper).

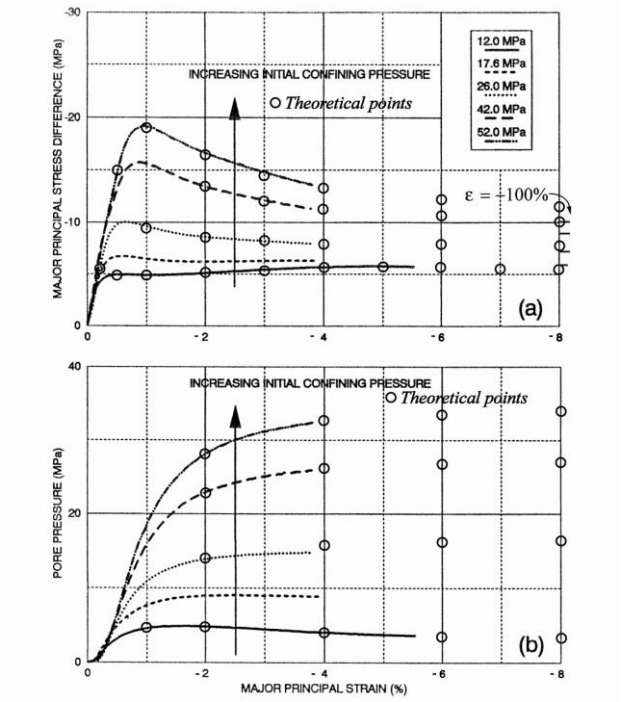

Figure 9. Undrauned Estension Tests Between 12.0 and 12.0 MPa Initial Confining Pressures on Dense Cambria Sand: (a) Principal Stress Difference; and (b) Pore Pressure Relations (from Lade and Yamamuro. 1996)

The 12.0 MPa test initially shows a tendency for volumetrically compressive behavior, but further shearing allows it to exhibit dilatant volumetric tendencies, as shown by the pore pressure variations depicted in Figure 9(b). The pore pressure initially increases and then later decreases, which causes the principal stress difference to decrease after its initial peak and then later to increase as the effective confining pressure

changes. For tests with initial confining pressures above 12.0 MPa, the maximum principal stress difference occurs at low strain values, because at the higher confining pressures, the specimens show increasing amounts of particle crushing resulting in continuously increasing pore pressures. Particle crushing is further discussed later. The major principal strain at the maximum principal stress difference increases slightly as the initial confining pressure increases. The tests exhibit declining principal stress differences after the maximum value is obtained."

"As discussed for undrained compression, the initial pore pressure response was slightly buffered due to volumetric creep occurring between isotropic compression and initiation of shearing."

For the third paper "Drained Sand Behavior in Axisymmetric Tests at High Pressures":

4.3 Isotropic compression

"An isotropic consolidation test was performed on dense Cambria sand to a confining pressure of 69.0 MPa, as shown on Figure 10. This diagram shows the volumetric strain related to the effective confining pressure for both the loading and unloading portions of the test. At a confining pressure of about 10 MPa, a dip appears on the loading branch of the curve. The cause of this dip has been identified as being related to the nature of the sand used in the testing. Cambria sand is composed of many mineral constituents of varying hardnesses. Some of the softer components consist of sedimentary lithic fragments (shale), which crush easily relative to the harder elements that are contained in the sand. The dip in the isotropic consolidation curve appears to coincide with confining pressures levels that occur after the softer components have been crushed leaving the harder elements intact. This phenomenon is explained in detail by Yamamuro and Lade (1993)."

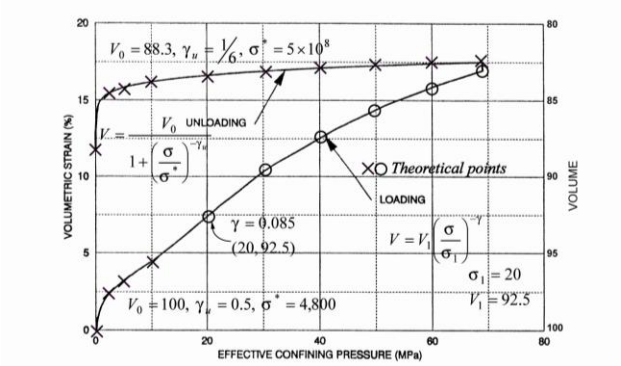

Figure 10. High-Pressure Isotropic Tests on Dense Cambria Sand (from Yamamuro and Lade. 1996)

4.4 Stress-strain and volume change behavior in compression

"A series of drained triaxial compression tests was performed on dense Cambria sand at various confining pressures between 2.1 and 52.0 MPa to establish the shape of the drained failure envelope in compression over a wide range of confining pressures, and to observe the overall stress-strain and volume change behavior in triaxial compression."

"Figures 11 (a) and 12 (a) show the normalized compression stress-strain characteristics of dense Cambria sand for the confining pressures shown. The effective principal stress ratios (σ_1/σ_2) are plotted against axial strain ε_1. The effective principal stress ratio is used so that variations in the shapes of the stress-strain curves can be examined conveniently over the wide confining pressure ranges employed in this study. This representation of the stress-strain curve is different from the true stress-strain curve, because the normalization by the effective minor principal stress creates flatter initial slopes with increasing confining pressures, rather than increasing initial moduli that the true stress-strain curves would indicate. The volumetric strains for the same tests are given on Figures 2(b) and 3(b) for dense Cambria sand."

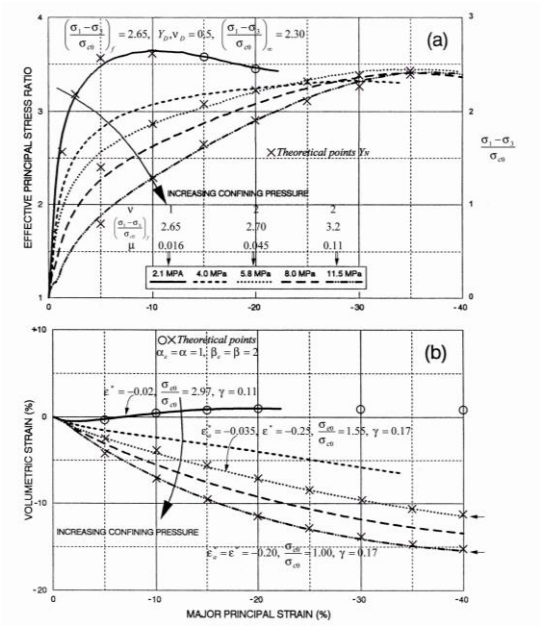

Figure 11. Compression Tests between 2.1 and 11.5 Mpa Confining pressures for Dense Cambria Sand: (a) Effective Principal Stress Ratio; and (b) Volumetric Strain Relations (from Yamamuro and Lade. 1996)

4.5 Stress-strain and volume change behavior in extension

4.5.1 Uniform Strain Extension Test Results

"A series of drained, uniform strain, triaxial extension tests was performed on dense Cambria sand at constant confining pressures between 0.25 and 52.0 MPa. All extension tests were conducted using the method depicted in Figure 13 to enforce uniform strains in extension. Tests using confining pressures below 2.2 MPa were conducted in a conventional low-pressure triaxial cell."

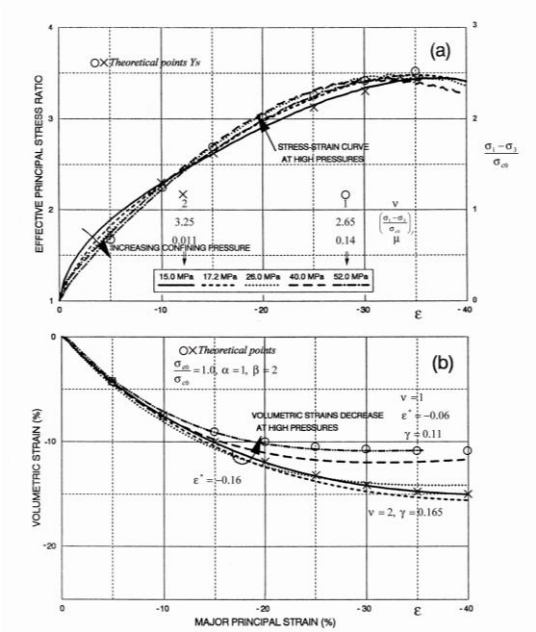

Figure 12. Compression Tests between 15.0 and 52.0 Mpa Confining pressures for Dense Cambria Sand: (a) Effective Principal Stress Ratio; and (b) Volumetric Strain Relations (from Yamamuro and Lade. 1996)

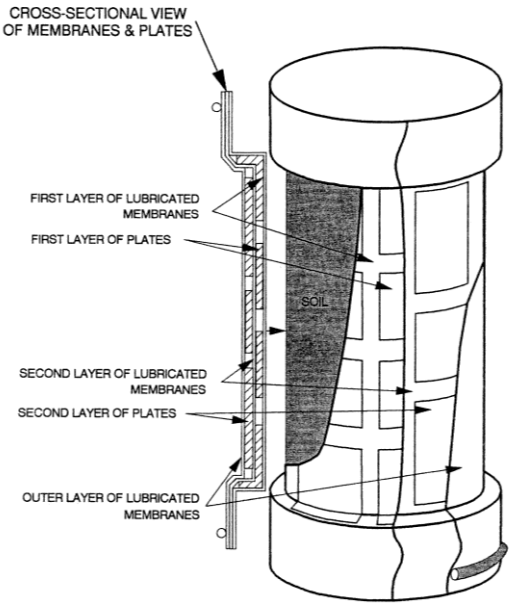

Figure 13. Method Developed to Enforce Uniform Strain Conditions in Cylindrical Triaxial Extension Specimens (from Yamamuro and Lade. 1996)

"The drained extension stress-strain characteristics are shown in Figures. 14 (a) and 15 (a), in which the effective principal stress ratio (σ'_1/σ'_3) is plotted against the major principal strain ε_1 or radial strain in the specimen. In general, the results indicate trends that are similar in nature to the drained compression tests previously discussed. In extension tests confining pressure is the major principal stress σ_1. As the confining pressure increases, the slopes of the normalized stress-strain curves decrease, the maximum effective principal stress ratios decrease, and the major principal strains at failure increase. The maximum effective stress ratio continues to decline with increasing confining pressure until the 14.5 MPa test is reached. At this confining pressure the effective stress ratio appears to stabilize at a minimum level, and it remains relatively constant throughout the remainder of the confining pressure range used in the experimental program. There tends to be more natural inherent scatter in the results of extension tests that in compression tests (Yamamuro and Lade. 1995), and this is reflected in the stress-strain behavior. The constant value of maximum effective stress ratio observed at the highest pressures is slightly lower than that obtained from he corresponding triaxial compression tests. At higher pressures the shapes of extension test stress-strain curves [Figure 15 (a)] begin to resemble the flattened shape of the higher pressure compression test curves, thus indicating large amounts of particle crushing in extension tests as well. The major principal strains at failure are seem to become relatively constant at higher confining pressures. The volumetric strains are displayed on [Figures. 14 (b) and 15 (b)]. The low-pressure tests indicate strong dilatant tendencies. As with the compression tests, the volume changes become more contractive as the confining pressure increases, and at very high confining pressures, the volumetric strains become highly contractive, corresponding to apparent negative Poisson's ratios. At higher confining pressures the volumetric strains at failure become approximately constant."

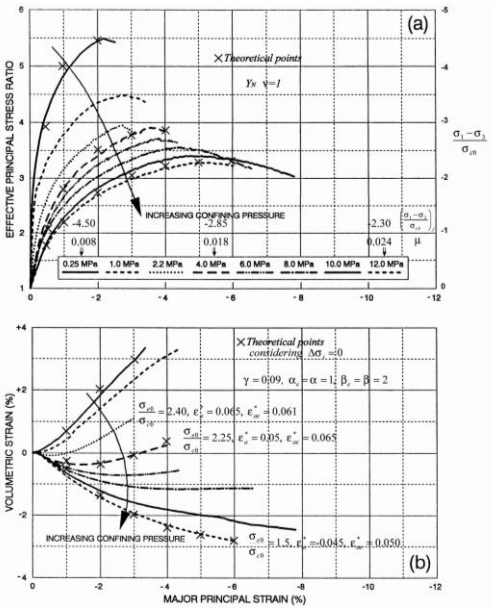

Figure 14. Extension Tests between 0.25 and 12.0 Mpa Confining pressures for Dense Cambria Sand: (a) Effective Principal Stress Ratio; and (b) Volumetric Strain Relations (from Yamamuro and Lade. 1996)

"Some of the extension tests also exhibit a slightly buffered volumetric strain response at the onset of shearing as did some of the compression tests. This was explained as being caused by volumetric creep occurring between the stages of isotropic compression and shearing."

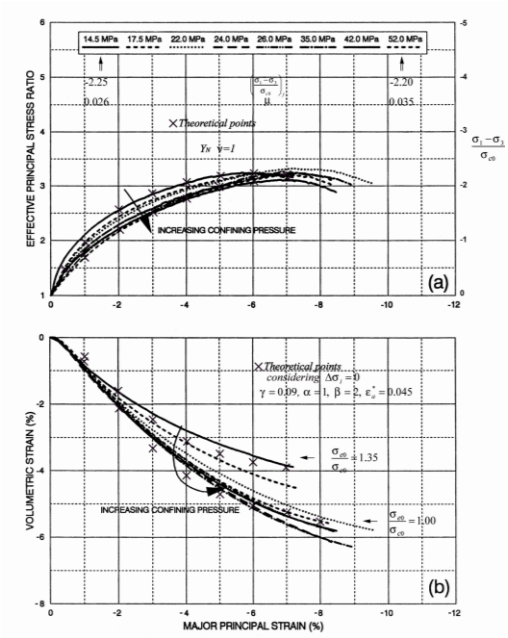

Figure 15. Extension Tests between 14.5 and 52.0 Mpa Confining pressures for Dense Cambria Sand: (a) Effective Principal Stress Ratio; and (b) Volumetric Strain Relations (from Yamamuro and Lade. 1996)

5 THEORETICAL EQUATIONS

The general theoretical equation of compressibility for geomaterials provided by the principle of natural proportionality reads (Juárez-Badillo. 1981)

$$V = \frac{V_0}{1+\left(\frac{\sigma}{\sigma^*}\right)^{\gamma}} \qquad [1]$$

where V = volume, σ = pressure, V_0 = volumen at $\sigma = 0$, σ^* = characteristic σ at $V = V_0/2$ and γ = natural coefficient of compressibility.

Equation [1] is for the unvirgin zone of compression. For the virgin zone of compression where $V_0 = \infty$ at $\sigma = 0$ Equation [1] reduces to

$$V = V_1\left(\frac{\sigma}{\sigma_1}\right)^{-\gamma} \qquad [2]$$

where (σ_1, V_1) is a known point.

In terms of void ratios equation [1] reads

$$e = \frac{1+e_0}{1+\left(\frac{\sigma}{\sigma^*}\right)^{\gamma}} - 1 \qquad [3]$$

and Equation [2] reads

$$e = (1+e_1)\left(\frac{\sigma}{\sigma_1}\right)^{-\gamma} - 1 \qquad [4]$$

When using both equations, unvirgin and virgin, the unvirgin coefficient of compressibility is denoted by γ_u.

The general theoretical equations for stress-strain, pore pressure and volume change provided by the principle of natural proportionality applicable to the experimental data are (Juárez-Badillo 1985, 1999a, b, 2005).

The pre-peak normal function Y_N with $\nu = 1$

$$\frac{\sigma_1-\sigma_3}{\sigma_{co}} = \left(\frac{\sigma_1-\sigma_3}{\sigma_{co}}\right)_f \left\{1-\exp\left[\frac{3e_a}{\mu\left(\frac{\sigma_1-\sigma_3}{\sigma_{co}}\right)_f}\right]\right\} \qquad [5]$$

where σ_{co} = initial confining pressure, $(\sigma_1-\sigma_3)$ = major principal stress difference, e_a = axial natural strain, $(\sigma_1-\sigma_3)_f$ = final $(\sigma_1-\sigma_3)$ at $e_a = \infty$ and μ = shear coefficient. The axial natural strain e_a in terms of the common strain (Cauchy) ε_a is given by

$$e_a = \ln(1+\varepsilon_a) - \frac{\varepsilon_v}{3} \qquad [6]$$

where ε_v is the natural volumetric strain, which in turn is given by

$$\varepsilon_v = \ln(1+\varepsilon_{vc}) \qquad [7]$$

where ε_{vc} is the common volumetric strain. Observe that in compression triaxial tests ε_a and e_a are negative and that ε_{vc} and ε_v are negative in decreasing volume. In undrained tests $\varepsilon_v = 0$.

The pre-peak normal function Y_N with $\nu = 2$

$$\frac{\sigma_1-\sigma_3}{\sigma_{co}} = \left(\frac{\sigma_1-\sigma_3}{\sigma_{co}}\right)_f \left\{1-\left[1-\frac{3e_a}{\mu\left(\frac{\sigma_1-\sigma_3}{\sigma_{co}}\right)_f}\right]^{-1}\right\} \qquad [8]$$

The pre-peak sensitivity function Y_s

$$\frac{\sigma_1-\sigma_3}{\sigma_{co}} = \left(\frac{\sigma_1-\sigma_3}{\sigma_{co}}\right)_f \left[1+\left(\frac{e_a}{e_a^*}\right)^{-\frac{1}{\nu}}\right]^{-1} \qquad [9]$$

where ν = shear exponent, $(\sigma_1-\sigma_3)_f$ = final $(\sigma_1-\sigma_3)$ at $e_a = \infty$ and e_a^* = characteristic e_a at $(\sigma_1-\sigma_3)=1/2(\sigma_1-\sigma_3)_f$.

The post-peak ductility function Y_D

$$\frac{\sigma_1-\sigma_3}{\sigma_{co}} = \left(\frac{\sigma_1-\sigma_3}{\sigma_{co}}\right)_\infty + \left[\left(\frac{\sigma_1-\sigma_3}{\sigma_{co}}\right)_1 - \left(\frac{\sigma_1-\sigma_3}{\sigma_{co}}\right)_\infty\right]\left(\frac{e_a}{e_{a1}}\right)^{-\frac{1}{\nu}} \qquad [10]$$

where $((\sigma_1-\sigma_3)/\sigma_{co})_\infty = ((\sigma_1-\sigma_3)/\sigma_{co}$ at $e_a = \infty$, ν = ductility coefficient and $[e_{a1}, (\sigma_1-\sigma_3/\sigma_{co})_1]$ is a known point.

The pore pressure equation

$$\Delta u = \Delta\sigma_i + \alpha\,\sigma_{co}Y - \alpha_e(\sigma_{eo}-\sigma_{co})Y_e \qquad [11]$$

where $\Delta\sigma_i$ = increment of isotropic component of the applied stresses, σ_{eo} = initial equivalent consolidation

pressure due to interlocking of the solid particles, Y = sensitivity function given by

$$Y = \left[1 + \left(\frac{e_a}{e_a^*} \right)^{-\beta} \right]^{-1} \qquad [12]$$

where β = a constant and e_a* characteristic e_a at Y=1/2, α and β = pore pressure parameters. Y_e, α_e, β_e have the small e (subscript e) just to distinguish them from the corresponding symbols of the second term.

The volume change equation

$$\frac{V}{V_o} = \left[1 + \frac{\Delta\sigma_i}{\sigma_{co}} + \alpha\, y - \alpha_e \left(\frac{\sigma_{eo}}{\sigma_{co}} - 1 \right) Y_e \right]^{-\gamma} \qquad [13]$$

Equation [13] was applied to the experimental data in drained tests in the form:

$$\frac{\Delta V}{V_o} = \frac{V}{V_o} - 1 \qquad [14]$$

Figures 16, 17, 18 and 19 present graphs at Y_N, Y_S, Y_D and Y.

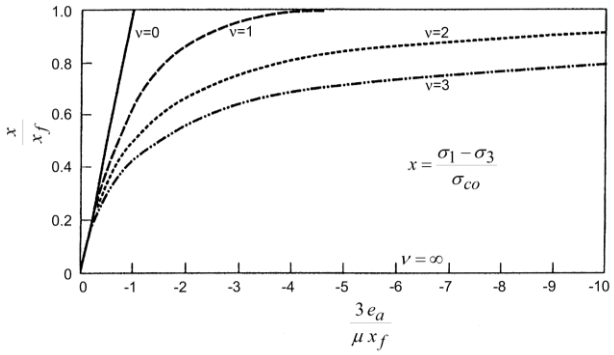

Figure 16. Prepeak normal function Y_N

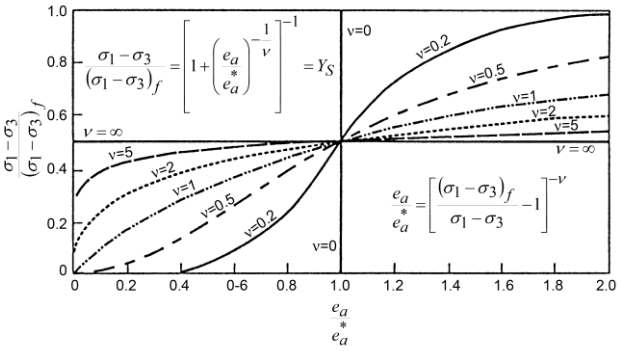

Figure 17. Prepeak sensitivity function Y_S

6 PRACTICAL APPLICATION

Equation [2] was applied to Figures 2, 3 and 4. The parameter values appear in these figures.

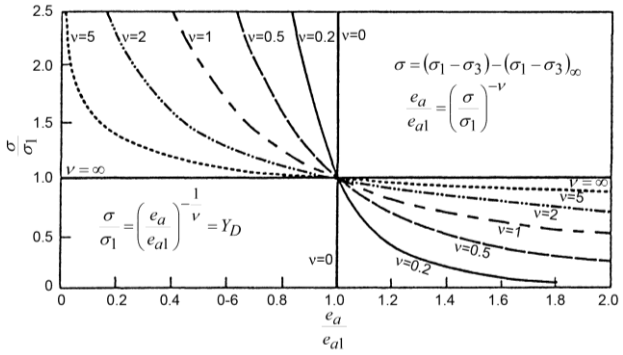

Figure 18. Postpeak ductility function Y_D

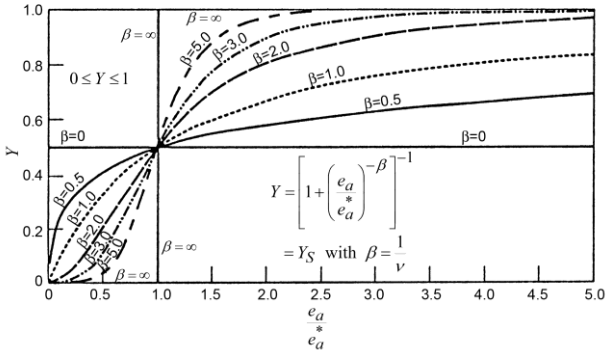

Figure 19. Sensitivity function Y

Equation [3] and [4] were applied to Figures 5, 6 and 7. The parameter values appear in these figures. Different symbols are used for the recompression zones (unvirgin), virgin zones and swelling zones. Important observations are: In the recompression zones the common values $\gamma_u = 1$ is observed for all three sands while σ^* increases with density of the sands. In the virgin zones the common values of $\gamma = 0.09$ and 0.10 appear in these figures in pressures from about 10 to 100 MPa while for pressures from about 100 to 850 MPa the values of γ are somewhat smaller and are identical to the values of Figures 2, 3 and 4. Important observation is that the transition from unvirgin zone to virgin zone increase with the hardness of the sand and in each sand the transition increases somewhat with the density of the sand. For pressures greater than about 1,000 MPa the void ratios will be less than 0 and will tend to e = -1 (V = 0) at very high pressures where the internal pressures i of the substances will play an important play (Juárez-Badillo and Hernandez-Mira. 2006). Values of γ_u greater that 1 are not very common; concrete has $\gamma_u = 2$ in the unvirgin zone and later on continues with Equation 2 in the virgin zone (Juárez-Badillo. 1985).

In all the undrained tests Equation [6] was used.

Figure 8 shows the theoretical points obtained from the theoretical equations for the undrained compression tests. The pre-peak normal function Y_N with $\nu = 1$ [5] was only applied to the test with $\sigma_{co} = 68.9$ MPa with $(\sigma_1-\sigma_3)_f = 31$ MPa and $\mu = 0.06$. For smaller σ_{co} the values of $(\sigma_1-\sigma_3)_f$ will be smaller. See Table 1.

Table 1. Parameter values for Undrained Compression Tests

σ_{co}	Pre-peak $Y_N\ (\nu=1)$		Post-peak, $Y_D\ (\nu=1)$			Pore Pressure		
	$(\sigma_1-\sigma_3)_f$	μ	ε_1	$(\sigma_1-\sigma_3)_\nu$	$(\sigma_1-\sigma_3)_\infty$	α	β	ε_a^*
MPa	MPa			MPa	MPa			
6.4	-	-	-0.20	6.0	2.8	0.50	2	-0.02
16.7	-	-	-0.20	6.5	4.8	0.75	2	-0.02
34.0	-	-	-0.10	10.2	9.0	0.85	2	-0.02
43.0	-	-	-0.10	12.3	10.5	0.85	2	-0.02
52.0	-	-	-0.10	14.7	12.0	0.85	2	-0.02
61.6	-	-	-0.10	17.8	15.0	0.85	2	-0.02
68.9	31	0.06	-0.10	21.8	18.0	0.82	2	-0.02

The post-peak ductility function Y_D [10] was applied to all the undrained compression tests with the parameter $\nu = 1$ and for $\sigma_{co} = 6.4$, 16.7 MPa $\varepsilon_1 = -0.20$ and for $\sigma_{co} = 34.0$, 43.0 52.0, 61.6 and 68.9 MPa $\varepsilon_1 = -0.10$ with values of $(\sigma_1-\sigma_3)_1$, from $\sigma_{co} = 6.4$ to $\sigma_{co} = 68.9$ equal to $(\sigma_1-\sigma_3)_1 = 6.0$, 6.5, 10.2, 12.3, 14.7, 17.8, 21.8 MPa and corresponding values of $(\sigma_1-\sigma_3)_\infty$ equal to $(\sigma_1-\sigma_3)_\infty = 2.8$, 4.8, 9, 10.5, 12, 15 and 18 MPa. See Table 1.

The pore pressure equation [11] was applied to all undrained compression tests in their post-peak zone with $\alpha_e = 0$, $b = 2$ and $\varepsilon_a^* = -0.020$ to all the tests. The values of α from $\sigma_{co} = 6.4$ to 68.9 MPa were $\alpha = 0.50$, 0.75, 0.85 and 0.82. The smaller values of α at $\sigma_{co} = 6.4$ to 16.7MPa very surely was because some value of σ_{eo} due to interlocking was acting that I did not disclosed explicitely. See Table 1.

Figure 9 shows the theoretical points obtained from the theoretical equations for the undrained extension tests. The pre-peak normal function Y_N with $\nu = 1$ [5] was only applied to the test with $\sigma_{co} = 52$ MPa with $(\sigma_1-\sigma_3)_f = -21$ MPa and $\mu = 0.06$. For this case the author obtained the axial common strains ε_a from radial common strains $\varepsilon_r = \varepsilon_1$ used in the tests using the approximate formula

$$\varepsilon_a = -2\varepsilon_r \qquad [15]$$

The post-peak ductility function Y_D [10] was applied to the undrained extension tests with the parameter $\nu = 1$, $\varepsilon_1 = -0.02$ to the cases of $\sigma_{co} = 26.0$, 42.0 and 52.0 MPa with values of $(\sigma_1-\sigma_3)_1 = -8.5$, -13.5 and -16.5 MPa respectively and corresponding values of $(\sigma_1-\sigma_3)_\infty = -7.5$, -9 and -10 MPa. For the case of $\sigma_{co} = 12.0$ MPa was applied a combination of the function Y_D (10) with the pre-peak sensitivity function Y_S (9), Y_D+Y_S with the following values of the parameters; for Y_D only $(\sigma_1-\sigma_3)_\infty = -5$ MPa was necessary since $(\sigma_1-\sigma_3)$ did not showed decreasing zone and for Y_S the values were $\nu=0.5$, $(\sigma_1-\sigma_3)_f = -1$ MPa and $\varepsilon_a^* = 0.06$ ($\varepsilon_1 = -0.03$). See Table 2.

Table 2. Parameter values for Undrained Extension Tests

σ_{co}	Pre-peak $Y_N\ (\nu=1)$		Post-peak, $Y_D\ (\nu=1)$			$Y_S\ (\nu=0.5)$		Pore Pressure						
	$(\sigma_1-\sigma_3)_f$	μ	ε_1	$(\sigma_1-\sigma_3)_\nu$	$(\sigma_1-\sigma_3)_\infty$	$(\sigma_1-\sigma_3)_f$	ε_a^*	α	β	ε_a^*	α_e	β_e	ε_{ae}^*	σ_{eo}
MPa	MPa			MPa	MPa	MPa								MPa
12.0	-	-	-	-	-5.0	-1.0	0.06	0.73	2	-0.005	0.73	2	-0.025	17
17.6	-	-	-	-	-	-	-	-	-	-	-	-	-	-
26.0	-	-	-0.02	-8.5	-7.5	-	-	0.73	2	-0.007	-	-	-	-
42.0	-	-	-0.02	-13.5	-9.0	-	-	0.73	2	-0.007	-	-	-	-
52.0	-21.0	0.06	-0.02	-16.5	-10.0	-	-	0.73	2	-0.007	-	-	-	-

The pore pressure equation [11] was applied to the above cases of σ_{co}=12.0, 26.0, 42.0, and 52.0 MPa. For all four cases it was obtained $\alpha = 0.73$ and $\beta = 2$. For the last three cases σ_{co} = 26.0, 42.0 and 52.0 MPa $\alpha_e = 0$ and $\varepsilon_a^* = -0.007$ and for the first case σ_{co} = 12.0 MPa, $\varepsilon_a^* = -0.005$ and $\alpha_e = 0.073$, $\beta_e = 2$, $\varepsilon_{ae}^* = -0.025$ and σ_{eo} = 17 MPa, showing interlocking of the solid particles. See Table 2.

Figure 10 shows the theoretical points from the theoretical equations of compressibility [1] and [2]. In the loading we have first the unvirgin zone from 0 to around 10 MPa to follow with the virgin zone. In unloading equation [1] was applied. The theoretical parameters are shown in this Figure. This Figure already is of the original third paper of drained tests.

Figures 11 (a) and 12 (a) show the theoretical points of the application of Equations [5], [8] and [10] to the compression tests indicated. In all the tests equation [6] was used. The values of the different parameters are shown in these Figures. Observe that for σ_{co} = 2.10 MPa the pre-peak behavior was with Y_N ($\nu = 1$) because particle crushing was not important and the post-peak behavior was with Y_D ($\nu = 0.5$). For σ_{co} = 5.8, 11.5 and 15.0 MPa the pre-peak behavior was with Y_N ($\nu = 2$) because particle crushing was important. For σ_{co} = 52.0 MPa the pre-peak behavior returned to be with Y_N ($\nu = 1$) very surely because the remaining particle crushing was not very important. In the application of Equation [6], equation [7], for simplicity, was not taking account, since for ε_{vc} = -10% and -15% the corresponding values of ε_v are ε_v = -10.54% and -16.25% and 1/3 ε_{vc} = -3.33% and -5.0% compared with 1/3 ε_v = -3.51% and -5.42%. So the error in general was small.

Figures 11 (b) and 12 (b) show the theoretical points of the application of Equation [12], [13] and [14] to the volumetric strains. The values of the different parameters are shown in these Figures. Observe that when particle crushing was not important for σ_{co} = 2.10 and 52.0 MPa the value of the natural compressibility coefficient was $\gamma = 0.11$ while when the particle crushing was important its value increases to $\gamma = 0.17$. Also observe that at σ_{co} = 2.10 MPa the interlocking of solid particles had a value of σ_{eo}/σ_{co} = 2.97 but at $\sigma_{co} \geq 11.5$ MPa the interlocking was null with $\sigma_{eo}/\sigma_{co} = 1$. Observe also that in these tests $\alpha_e = \alpha = 1$ and $\beta_e = \beta = 2$.

Figures 14(a) and 15(a) show the theoretical points of the application of Equation [5] to the extension tests indicated. The values of the different parameters are shown in these figures. Observe that in these tests the particle crushing was not important since all tests were with Y_N ($\nu = 1$). For this case the author obtained the axial common strains ε_a from the radial common strain $\varepsilon_r = \varepsilon_1$ using in these tests the approximate formula defined by Equation [15].

Figures 14(b) and 15(b) show the theoretical points of the application of Equations [12], [13] and [14] to the volumetric strains. The values of the different parameters are shown in these Figures. Observe that as the extension tests were made decreasing the axial stress (if they would had been done increasing the radial stresses the history would be different) and as the natural swelling coefficient in sands is small compared to the natural compressibility coefficient γ, the decrease in isotropic component σ_i of the applied stresses was ignored, that is, was considered that $\Delta\sigma_i = 0$. So all volumetric strain was considered to be due to σ_{co} and to σ_{eo}. We may observe that for these tests we have general values of $\gamma = 0.09$, $\alpha_e = \alpha = 1$ and $\beta_e = \beta = 2$ and that the values of the particle interlocking for σ_{co} = 0.25 MPa, σ_{eo}/σ_{co} = 2.40 to $\sigma_{eo}/\sigma_{co} = 1$ for σ_{co} = 52.0 MPa.

7 CONCLUSIONS

For the first paper “One-Dimensional Compression of Sand t High Pressures”:

In the three sands tested at three different initial void ratios Equation [1] duplicated the experimental data in the unvirgin zone with $\gamma_u = 1$ and σ^* increasing with initial density of the sands. Equation [2] duplicated the experimental data with $\gamma = 0.09$ and $\gamma = 0.10$ to pressures up around 100 MPa and with values somewhat smaller up to 850 MPa. When the void ratio approaches 0 the internal pressure *i* of the substances will play an important role when the void ratios varies from 0 to -1 ($V = 0$).

For the second paper “Undrained Sand Behavior in Axisymmetric Tests at High Pressures”, the main conclusions are:

1. The pre-peak undrained compression and extension tests are described by the pre-peak normal function Y_N with $\nu = 1$, Equation [5], Figure 16.
2. The post-peak undrained compression and extension tests are described by the post-peak ductility function Y_D with $\nu = 1$, Equation [10], Figure 18.
3. The post-peak undrained compression at low pressures σ_{co} = 6.4 and 16.7 MPa and the undrained extension at σ_{co} = 12.0 and 17.6 MPa, show the influence of interlocking of the solid particles and are described by the post-peak ductility function Y_D with $\nu = 1$ plus the pre-peak sensitivity function Y_s with $\nu = 5$; however this was only calculated for the case of undrained extension test with σ_{co} = 12.0 MPa, Equation [9], Figure 17.
4. The pore pressure in undrained compression tests are described with values of $\beta = 2$ and $\varepsilon_a^* = -0.02$ and $\alpha = 0.85$ except at low values of σ_c = 16.7 and 6.4 MPa where $\alpha = 0.75$ and 0.50 due to interlocking of the solid particles, interlocking that was not disclosed explicitely in these cases.
5. The pore pressure in undrained extension tests are describe with values of β=2 and $\varepsilon_a^* = -0.007$ and $\alpha = 0.73$ for the cases σ_{co} = 26.0, 42.0, and 52.0 MPa. The case of σ_{co} = 12.0MPa that showed interlocking of solid particles, the values found were $\alpha_e = \alpha = 0.73$, $\beta_e = \beta = 2$, $\varepsilon_a^* = -0.005$ $\varepsilon_{a_e}^* = -0.025$ and σ_{eo} = 17 MPa.

For the third paper: “Drained Sand Behavior in Axisymmetric Tests at High Pressures”, the main conclusions are:

1. In the compression tests with σ_{co} = 2.1 and 52.0 MPa and in all the extension tests the pre-peak behavior was with Y_N ($\nu = 1$) because the particle crushing was not important. In the compression tests with

σ_{co} = 5.8 to 15 MPa the behavior was with Y_N (ν = 2) because the particle crushing was important.

2. In the compression tests with σ_{co} = 2.1 MPa the post-peak behavior was with the post-peak ductility function Y_D (ν = 0.5).

3. The volumetric strains in compression tests showed at σ_{co} = 2.1 MPa interparticle interlocking with a value σ_{eo}/σ_{co} = 2.97 but disappeared for $\sigma_{co} \geq$ 11.5 MPa where σ_{eo}/σ_{co} = 1.

4. The natural coefficient of compressibility in compression test was γ = 0.11 when the particle crushing was not important but it increased to γ = 0.17 when the particle crushing was important. In the extension tests its value was γ = 0.09.

5. In all the compression and extension tests have common values of $\alpha_e = \alpha = 1$ and $\beta_e = \beta = 2$. In general de values of Y_e and Y were different with different values of the characteristic strains ε_{ae}* and ε_a*.

8 ACKNOWLEDGMENTS

The author is very grateful to Mrs. Juliana Constanza Zapata-Chica and Mr. Sergio Hernández-Mira for their assistance in the preparation of this paper.

9 REFERENCES

Juárez–Badillo, E. 1981. General compressibility equation for soils. In *Proceedings of X Int. Conf. on Soil Mech. and Found. Engng.* Stockholm, 171-178.

Juárez-Badillo, E. 1985. General volumetric constitutive equation for geomaterials. Special volume in Constitutive Laws of Soils. In *Proceedings of XI International Conference on Soil Mechanics and Foundation Engineering,* San Francisco. Japanese Society for Soil Mechanic and Foundation Engineering, Tokyo, pp. 131-135.

Juárez–Badillo, E. 1999a. Static liquefaction of very loose sands: Discussion. *Canadian Geotechnical Journal* 36(5): 967-973.

Juárez–Badillo, E. 1999b. Static liquefaction of sands under multiaxial loading: Discussion. *Canadian Geotechnical Journal* 36(5): 974-979.

Juárez-Badillo E. 2005. Fraser River sand. Mathematical characterization. In *Proceedings of 16 th. Int. Conf. Soil Mech. and Geotech. Engng.*, Osaka (2): 391-396.

Juárez-Badillo, E. and Hernández-Mira, S. 2006. Mathematical Characterization of the Compression to 45,000 kg/cm^2 of Fourteen Substances. In *Proceedings of Int. Conf. on New Developments in Geoenvironmental and Geotech. Engng.* Incheon, Korea, 154-161.

Lade, P.V. and Yamamuro, J. A. 1996. Undrained San Behavior in Axisymmetric Tests at High Pressures. *Journal of Geotechnical Engineering* 122(2): 120-129.

Yamamuro, J. A., Bopp, P.A. and Lade, P.V. 1996. One-Dimensional Compression of Sands at High Pressures. *Journal of Geotechnical Engineering* 122(2): 147-154.

Yamamuro, J. A. and Lade, P.V. 1996. Drained San Behavior in Axisymmetric Tests at High Pressures. *Journal of Geotechnical Engineering* 122(2): 109-119.